Bone 198 (2025) 117539

Contents lists available at ScienceDirect

Bone

journal homepage: www.elsevier.com/locate/bone

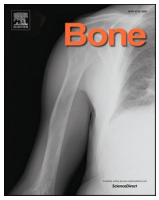

Full Length Article

The role of the extracellular matrix protein SPOCK2 for bone physiology and hematopoiesis

Rahul Kumar [a], Subhadeep Das [a], Wahyu Minka [b], Celina Reiter [c], Raquel Pereira [d], Dominik Fuhrmann [e], Richard Schneider [f], Anita Seshire [f], Christof Reusch [f], Claire Conche [g], Katharina Imkeller [h,i,j], Paola Divieti Pajevic [k,1], Daniela S. Krause [a,l,m,n,*,1]

[a] Institute of Transfusion Medicine – Transfusion Center, Johannes Gutenberg University Medical Center, 55131 Mainz, Germany
[b] Evotec International GmbH, 37079 Göttingen, Germany
[c] Georg-Speyer-Haus, 60596 Frankfurt am Main, Germany
[d] Institute for Experimental Pediatric Hematology and Oncology, Goethe-University Frankfurt, Frankfurt am Main, Germany
[e] Goethe University Frankfurt, University Hospital, Institute of Biochemistry I-Pathobiochemistry, 60596 Frankfurt am Main, Germany
[f] Merck Healthcare KGaA, 64293 Darmstadt, Germany
[g] The Helmholtz Institute for Translational Oncology Mainz (HI-TRON Mainz), Germany
[h] Goethe University Frankfurt, University Hospital, Edinger Institute (Neurological Institute), 60596 Frankfurt am Main, Germany
[i] University Cancer Center (UCT), 60596 Frankfurt am Main, Germany
[j] Frankfurt Cancer Institute, Frankfurt, Germany
[k] Boston University, Goldman School of Dental Medicine, Boston, MA 02118, USA
[l] Research Center for Immunotherapy (FZI), University Medical Center, University of Mainz, Mainz, Germany
[m] German Cancer Research Center (DKFZ), Heidelberg, Germany
[n] German Cancer Consortium (DKTK), Germany

ARTICLE INFO

Keywords:
Extracellular matrix
Bone marrow microenvironment
Bone
Hematopoiesis

ABSTRACT

The bone marrow microenvironment (BMM) consists of different cellular and acellular components. These components synergize in regulating the process of hematopoiesis. Various extracellular matrix proteins are found amongst the acellular components. Secreted protein acidic and rich in cysteine (SPARC) is amongst the most abundant glycoproteins in bone. Sparc/osteonectin, cwcv, and Kazal-like domains proteoglycan 2 (SPOCK2) is a member of the SPARC family, and its role in bone metabolism and hematopoiesis has not been investigated. Using female mice deficient for SPOCK2, we assessed the role of SPOCK2 in influencing bone formation, the BMM and hematopoiesis. Using micro-computed tomography we found a significant decrease in trabecular bone volume, bone mineral density and thickness, but increased cortical mineral density in SPOCK2 knockout (KO) versus wildtype (WT) bones. C-terminal telopeptide of type I collagen, a measure of bone resorption, was significantly increased in bone marrow supernatants of SPOCK2 KO mice. In the hematopoietic compartment we found an increase in hematopoietic stem cells, but a decrease of mesenchymal stromal cells and adipocytes in the bone marrow of SPOCK2 KO mice compared to control mice. Megakaryocytes were increased in SPOCK2 KO mice. In summary, deficiency of SPOCK2 leads to several alterations in the BMM. The hematopoietic effects may be due to hematopoietic cell-intrinsic effects in SPOCK2-deficient cells or due to a SPOCK2-deficient niche or both.

1. Introduction

The bone marrow microenvironment (BMM) is a complex system of both cellular and acellular components and represents the space, where hematopoiesis occurs. As part of hematopoiesis, hematopoietic stem cells (HSC) at the top of the hematopoietic hierarchy give rise to a

Abbreviations: BMM, Bone marrow microenvironment; HSC, Hematopoietic stem cells.

* Corresponding author at: Institute of Transfusion Medicine – Transfusion Center, Johannes Gutenberg University Medical Center, Building 900, Augustusplatz 4, 55131 Mainz, Germany.
E-mail address: krauseda@uni-mainz.de (D.S. Krause).

[1] These are co-senior authors.

https://doi.org/10.1016/j.bone.2025.117539
Received 5 October 2024; Received in revised form 17 May 2025; Accepted 18 May 2025
Available online 20 May 2025

variety of precursors and ultimately mature hematopoietic cells such as leukocytes, erythrocytes and platelets [1]. The process of hematopoiesis is governed by both cell-intrinsic and cell extrinsic cues [2]. The interplay of various components of the BMM such as cells, secreted proteins, extracellular matrix proteins, neurons etc. regulate HSCs and hence hematopoiesis [2,3]. Blood vessels in the BMM, such as sinusoids, arterioles or transition zone vessels in specific anatomical locations in the BM, contribute to the formation of distinct niches. While controversy remains about the exact nature of these niches, it is believed that active HSC responsible for the daily replenishing of blood cells are found in sinusoidal niches. In contrast, endosteal niches seem more relevant for the regenerative capacity of HSC [4,5]. Large focus has been placed on the cellular components and associated endothelial or endosteal niches in the BMM, but the role of acellular components such as the extracellular matrix (ECM) has been largely ignored.

In multicellular organisms, the ECM is a complex and dynamic network of molecules that surrounds and supports cells. The ECM represents a complex of proteins, such as collagen, elastin, fibronectin and laminin, as well as polysaccharides and other macromolecules like glycosaminoglycans or proteoglycans, all of which provide strength, elasticity and adhesive characteristics to the BMM and support of hematopoietic cells [6,7].

Secreted protein acidic and rich in cysteine (SPARC) or osteonectin represents a superfamily of matricellular proteoglycans whose role in homeostasis and disease is slowly being recognized. The proteins of this superfamily are structurally related, contain an acidic domain and are characterized by conserved cysteine-rich regions. SPARC family proteins may modulate cell-matrix interactions, tissue formation, and remodeling. They have various roles, including the regulation of cell adhesion, motility, proliferation and differentiation. SPARC proteins may also interact with other elements of the ECM, growth factors and cell surface receptors, which may impact a variety of biological processes [8,9]. SPARC is amongst the most abundant glycoproteins in bone, and SPARC KO mice have osteopenia and reduced collagen production [10].

Sparc/osteonectin, cwcv, and Kazal-like domains proteoglycan 2 (SPOCK2 or testican 2), a member of the SPARC superfamily, is expressed in kidney, heart and the skeletal system [11–13]. It is characterized by different domains, including the Kazal-like, the osteonectin-like, and the SPARC domains which interact with other elements of the matrix and cell surface receptors, which may impact cell adhesion, motility, and signaling [14]. Studies indicate that SPOCK2 may be involved in the processes of osteogenesis, angiogenesis and wound healing even if its precise roles are still not well understood [15]. In patients, SPOCK2 was identified as a potential susceptibility gene for hereditary bronchopulmonary dysplasia, with the lung expression pattern indicating a possible role in alveolarization [16].

In cancer, SPOCK2 may act as tumor suppressor or promoter of cancer growth. SPOCK2 expression has been linked to a good prognosis in some malignancies, including lung adenocarcinoma [17,18] and pancreatic ductal adenocarcinoma [19]. In contrast, SPOCK2 expression has been connected to more aggressive tumor activity and poor clinical outcomes in other cancer types, such as high grade serous ovarian cancer [20] and colorectal cancer [21].

Given the lack of more profound insight into the role of SPOCK2 for osteogenesis and hematopoiesis, we describe here the effects of SPOCK2 deficiency for these processes in a murine model. Overall, we find differences in bone density, mesenchymal stromal cell function and hematopoiesis, suggesting that the ECM protein SPOCK2 may be involved.

2. Materials and methods

2.1. Mice

SPOCK2 knockout (KO) mice (C57BL/6NTac background) were generated using CRISPR/Cas9-mediated gene editing (deletion of exon 1 and approximately 1.7 kb of sequence upstream of exon 1 (promoter region) to exon 4) of the *Spock2* gene (Fig. 1). Two different guide RNAs (gRNA) were selected (proximal guide RNA: CAACTTGATATGTAGCTTGA; distal guide: GATGCCTAATATGTAAGGAC) (based on their position and a low number of predicted off-targets. The strategy for targeting was based on NCBI transcript NM_052994.2.

After administration of hormones, superovulated C57BL/6NTac females were mated with C57BL/6NTac males. One cell-stage fertilized embryos were isolated from the oviducts at days post coitum (dpc) 0.5. For microinjection, the one cell-stage embryos were placed in a drop of M2 medium under mineral oil. A microinjection pipette with an approximate internal diameter of 0.5 mm (at tip) was used to inject the mixed nucleotide preparation, i.e. Cas9 protein along with the proximal and distal gRNAs, into C57BL/6NTac zygotes (the pronucleus of each embryo). After recovery, 25–35 injected one cell-stage embryos were transferred to one of the oviducts of 0.5 dpc, pseudopregnant NMRI females. A total of four animals were identified as valid founders (F0, KO/?). Identification of valid F0 included PCR amplification and subcloning of the PCR product for further characterization by sequencing, to allow assessment of the number of valid versus invalid modifications per animal. Two suitable males were selected for further breeding (Supplementary figs. 1 A-C).

For genotyping of the KO mice the following PCR primers were used: Forward primer: ACATTGTGGATAGCTTTGACTAGG, reverse primer 1: GTTACCACAGCACAAGGAACTG, reverse primer 2: CCACACATATATAGCATGCGATG. The KO band appears at 281 bp, while the WT band appears at 490 bp. Heterozygous animals (F1) were generated by using sperm of one of the F0 animals by in vitro fertilization (IVF). To allow the performing of IVF, F0 males were chosen as preferred sex. As two valid F0 males were identified in this model generation project, only one of them (male 2,180,680) was chosen to be used for the IVF based on sequencing and PCR data, in addition to health status.

The mice used for experiments were obtained by homozygous x homozygous HOM/HOM and WT (Wildtype) x WT matings. WT control mice (C57/BL6NTac) were obtained from Taconic. The age of the mice used for experiments varied between 7 and 12 weeks and female mice were used for the majority of experiments, unless stated otherwise. WT and SPOCK2 KO mice were age-matched per experiment. 4–5 mice were housed in one cage, and all mice were fed ad libitum with regular chow. All murine studies were approved by the local animal care committee (Regierungspräsidium Darmstadt) in Hessen, Germany.

2.2. Hematological analyses

SPOCK2 KO and WT C57/BL6 mice (7–12 weeks old) were sacrificed using CO_2 asphyxiation. Peripheral blood (PB) was taken from the vena cava inferior, and bones (femora) and spleens were harvested. Peripheral blood was analyzed using a Scil Vet animal blood counter (Scil Animal Care Company, Viernheim, Germany). Bones and spleens were crushed, and red blood cell lysis was performed using ACK lysis buffer (Cat. No. A1049201, Thermo Fisher Scientific, Waltham, MA, United States). Subsequently, samples were stained with the respective antibodies for flow cytometric analysis. The samples were analyzed on a BD Fortessa, Heidelberg, Germany. A list of all used antibodies can be found in Table 1.

2.2.1. Immunophenotypes

2.2.1.1. Hematopoietic stem and progenitor cells [22,23]. Lin- (lineage): $B220^-$, $Gr1^-$, $CD5^-$, $Ter119^-$, $F4/80^-$.

LKS: Lin^-, $c\text{-}Kit^+$, $Sca1^+$.

MPP: Lin^-, $c\text{-}Kit^+$, $Sca1^-$, $Flk2^+$, $Thy1.1^-$.

MPP2: Lin^-, $c\text{-}Kit^+$, $Sca1^-$, $Flk2^-$, $CD48^+$, $CD150^+$, $CD34^+$.

CLP: Lin^-, $cKit^{low}$, $Sca1^-$, $IL7R\alpha^-$, $Thy1.1^-$.

MEP: Lin^-, $cKit^+$, $Sca1^-$, $CD16/32^-$, $IL7R\alpha^-$.

CMP: Lin^-, $cKit^+$, $Sca1^-$, $CD16/32^-$, $IL7R\alpha^+$.

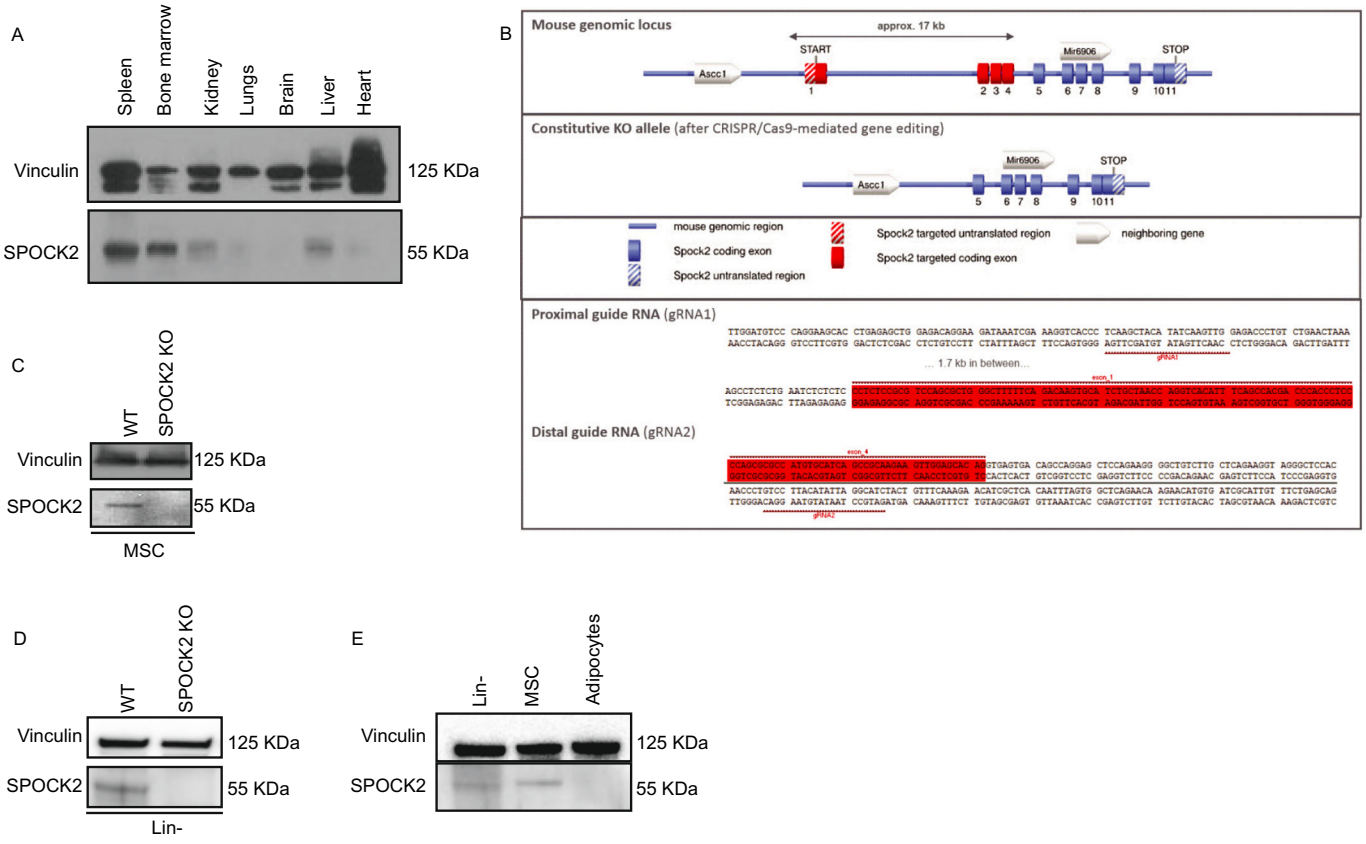

Fig. 1. A) Immunoblot showing the expression of SPOCK2 (55 kDa) and vinculin (125 kDa) as loading control in lysates of the respective organs of wildtype C57/BL6 mice. The image is representative of three independent immunoblots. B) Schematic showing the gene locus and proximal and distal guide RNAs for the CRISPR-CAS-mediated knockout of *Spock2* from the mouse genome. C-D) Immunoblots showing the expression of SPOCK2 (55 kDa) and vinculin (125 kDa) as loading control in lysates of MSC (C) and Lin$^-$ (hematopoietic) cells (D) from WT or SPOCK2 KO mice. The image is representative of three independent immunoblots per figure. E) Immunoblot showing the expression of SPOCK2 (55 kDa) and vinculin (125 kDa) as loading control in lysates of Lin$^-$ cells, MSC and adipocytes, which had been obtained by the in vitro differentiation of MSC, from WT mice. The image is representative of three independent immunoblots.

GMP: Lin$^-$, cKit$^+$, Sca1$^-$, CD16/32$^-$, IL7Rα$^{+\cdot}$

2.2.1.2. B cell progenitors [24]. Pre/Pro-B: B220^{low}, CD43^{High}, BP1$^-$, HSA$^-$.

Pro—B: B220^{low}, CD43^{High}, BP1$^-$, HSA$^+$.

Pre—B: B220^{low}, CD43^{High}, BP1^{High}, HSA$^+$.

Small Pre—B: B220^{High}, CD43$^-$, IgM$^-$.

Immature Pre—B: B220^{High}, CD43$^-$, IgM^{Mid}.

Mature Pre—B: B220^{High++}, CD43$^-$, IgM$^{High/Mid}$.

2.3. Nanostring analysis

Primary mesenchymal stromal cells (MSC) (PDGFRα$^+$, Sca1$^+$, Ter119$^-$, CD45$^-$) and HSC (Lin$^-$, Sca1$^+$, c-Kit$^+$) were flow sorted from crushed femora, tibiae and pelvis from WT or SPOCK2 KO mice and frozen in TRIzol (Cat. No. 15596026, Thermo Fisher Scientific, Waltham, MA, USA). For nanostring analysis, RNA was extracted from frozen cells using the RNAqueous-4PCR Kit or PureLink® (Thermo Fisher Scientific, Waltham, MA, USA). Purified RNA was quantified using a Qubit® 3.0 Fluorometer (Thermo Fisher Scientific, Waltham, MA, USA). Gene expression/amplification were tested using the multiplex digital nCounter® platform and analyzed with the NanostringApp (Merck Healthcare KGaA) and nSolver v4.0 software according to the manufacturer's instructions (NanoString Technologies, Inc., Seattle, WA, USA). Gene expression was analyzed using 1.4–16.9 ng of input RNA using the PanCancer Pathways Panel (NanoString), which contains 779 genes including the 29 customized genes from 13 canonical cancer-associated pathways. Raw counts in each sample were corrected by subtracting the mean + 2 standard deviations (SDs) from negative controls and then normalizing against the geometric means of both positive controls and reference genes. Expression levels were summarized as z-scores, which indicate the number of SDs by which the expression level differs from the mean.

Gene set enrichment analysis was performed on the differential gene expression results sorted according to the *stat* parameter calculated by DESeq2. We used mouse-specific pathway annotations from MsigDB [25] and the GSEA function of clusterProfiler [26].

2.4. TRAP staining

Femora were freshly isolated after sacrificing the WT and SPOCK2 KO mice. The bones were fixed overnight in formalin and then decalcified using 0.5 M EDTA for three weeks. The final step of decalcification was performed by shaking the bones at 37 °C for 24 h. Paraffin sections were subsequently prepared. Paraffin sections were initially deparaffinized and rehydrated with graded ethanol and finally with distilled water. Trap staining solution was prepared by using three components:

1. TRAP basic incubation medium (sodium acetate anhydrous (Cat. No. S-2889, Sigma-Aldrich, Darmstadt, Germany), L-(+) tartaric acid (Cat. No. T-6521, Sigma-Aldrich, Darmstadt, Germany), glacial acetic acid (Cat. No. A6283, Sigma-Aldrich, Darmstadt, Germany)
2. Fast red violet LB salt (Cat. no. F-3381120, Sigma-Aldrich, Darmstadt, Germany)
3. Napthol AS-MX phosphate substrate mix (Napthol AS-MX Phosphate (Cat. no. N-4875, Sigma-Aldrich, Darmstadt, Germany)) with

Table 1
Antibodies used in the study.

Antibody	Fluorochrome	Company	Catalogue number
Phalloidin	AlexaFluor 647	Life Technologies	A22287
Streptavidin	APC-Cy7	Biolegend, San Diego, CA	405208
CD48	Pacific blue	Biolegend, San Diego, CA	103413
CD150	Phycoerythrin (PE)	BD Biosciences, San José, CA	562651
Sca-1	Phycoerythrin -Cy7	Biolegend, San Diego, CA	108114
c-Kit	Allophycocyanin	BD Biosciences, San José, CA	553356
CD5-Biotin		BD Biosciences, San José, CA	553019
B220-Biotin		BD Biosciences, San José, CA	553086
F4/80-Biotin		eBiosciences, San Diego, CA	13–4801-82
Ly6G- and Ly6C-Biotin		BD Biosciences, San José, CA	553125
Ter119-Biotin		BD Biosciences, San José, CA	553672
Vinculin		Cell Signaling Technology, Danvers, Massachusetts, United States	4650
Gr-1	Allophycocyanin-Cy7	BD Biosciences, San José, CA	557661
CD11b	Allophycocyanin	BD Biosciences, San José, CA	553312
CD45R/B220	Pacific blue	Biolegend, San Diego, CA	103227
CD43	Phycoerythrin-Cy7	Biolegend, San Diego, CA	143210
CD24 (HSA)	APC	Biolegend, San Diego, CA	138506
CD49(BP-1)	FITC	eBIOSCIENCE, Frankfurt, Germany	11–5891-82
IgM	PerCP/ Cyanine5.5	Biolegend, San Diego, CA	406512
γH2AX antibody		Cell Signaling Technology, Danvers, Massachusetts, United States	9718
Alexa Fluor™ 647		Thermo Fisher Scientific, Waltham, MA, USA	A-21245
CD127 (IL7R α)	BV421	BD Biosciences, San José, CA	566377
CD90	PerCP	BD Biosciences, San José, CA	557266
FLK (CD135)	PE	Biolegend, San Diego, CA	135306
CD34	PE	Biolegend, San Diego, CA	119307
SPOCK2		Novus Biologicals, Centennial, CO	NBP1–92442

PE = Phycoerythrin; FITC = Fluorescein Isothiocyanate; BV=Brilliant Violet; APC = Allophycocyanin; Cy = Cyanine; PB=Pacific Blue, PerCP = Peridinin-Chlorophyll-Protein, Phycoerythrin-Cy7 = PE-Cy7.

ethylene glycol monoethyl ether (Cat. no. E-2632, Sigma-Aldrich, Darmstadt, Germany). Deparaffinized slides were then incubated with pre-warmed (37 °C) TRAP staining solution mix and incubated at 37 °C for 30–45 min. The slides were then washed with distilled water and counterstained using fast green (0.08 %) for 5 min. The slides were rinsed multiple times and finally air dried and mounted using mounting medium (Cat. No. 1.09016, Sigma-Aldrich, Darmstadt, Germany). The slides were evaluated using a light microscope (ECLIPSE Ts2, NIKON, Minato City, Tokyo, Japan).

2.5. Flow cytometry for reactive oxygen species and DNA damage

Intracellular ROS levels were measured using CellROX™ Deep Red Reagent (Cat. No. C10422, Thermo Fisher Scientific, Waltham, MA, USA). Briefly, cells were incubated with 200 nM of CellROX and incubated at 37 °C for 30 min. The cells were then centrifuged and resuspended in FACS buffer and detected using flow cytometry.

Table 2
Primers used in the study.

Primer	Sequence
Bglap (osteocalcin) fwd	5′-CCGGGAGCAGTGTGAGCTTA-3′
Bglap (osteocalcin) rev	5′- TAGATGCGTTTGTAGGCGGTC-3′
Tnfsf11 (TNF Superfamily Member 11; RANKL) fwd	5′- CACAGCGCTTCTCAGGAGCTC-3′
Tnfsf11 (TNF Superfamily Member 11; RANKL) rev	5′- GAGATCTTGGCCCAGCCTCGA-3′
Tnfrsf11b (osteoprotegerin) fwd	5′- AGGTTTAAACTCTCAAAGCTCCTG-3′
Tnfrsf11b (osteoprotegerin) rev	5′- GCCAGGAGCACATTTGTCAC-3′
Adipoq (adiponectin) fwd	5′- GGGAACTTGTGCAGGTTGGAT-3′
Adipoq (adiponectin) rev	5′- CTTAGGACCAAGAAGACCTGCATC-3′
Plin5 (perilipin 5) fwd	5′- CCAGGAACAGCATCAGTGTG-3′
Plin5 (perilipin 5) rev	5′- CTGCTGTCTCTTTGGCCATC-3′
Pparg (PPAR gamma) fwd	5′ -GGGGATGTCTCACAATGCCA-3′
Pparg (PPAR gamma) rev	5′ -ATCTCCGCCAACAGCTTCTC-3′
Pdk1 (pyruvate dehydrogenase kinase 1) fwd	5′ -CCACTGAGGAAGATCGACAGAC-3′
Pdk1 (pyruvate dehydrogenase kinase 1) rev	5′ -AGAGGCGTGATATGGGCAATCC-3′
Tnf (tumor necrosis factor) fwd	5′ -GATCGGTCCCCAAAGGGATG-3′
Tnf (tumor necrosis factor) rev	5′ -GGCTACAGGCTTCTCACTCG-3′
Gapdh (glyceraldehyde-3-phosphate dehydrogenase) fwd	5′ -AGGTCGGTGTGAACGGATTTG-3′
Gapdh (glyceraldehyde-3-phosphate dehydrogenase) rev	5′ -GGGGTCGTTGATGGCAACA-3′

fwd = forward; rev = reverse.

For measuring DNA damage the cells were centrifuged and permeabilized using 4 % paraformaldehyde (Cat. No. CAS30525–89-4, Santa Cruz Biotechnology, Dallas, Texas, United States) for 20 min. After washing the cells with FACS buffer, the cells were stained with the γH2AX antibody for one hour. The cells were then washed and stained with the secondary antibody against γH2AX (anti-Rabbit Alexa Fluor™ 647, Table 1). After one hour of incubation, cells were washed again and DNA damage was detected using flow cytometry.

2.6. Isolation of mesenchymal stromal cells (MSC)

MSC ($PDGFR\alpha^+$, $Sca1^+$, $Ter119^-$, $CD45^-$) were isolated from the femora, tibiae and pelvis of WT and SPOCK2 KO mice, as previously described [27]. Briefly, long bones from mice were cut into fine pieces and treated with 0.1 % collagenase type I (Cat. No. 05172969103, Roche, Basel, Switzerland) for one hour at 37 °C. Samples were then crushed again. The supernatant was collected and centrifuged. The cell pellet was resuspended in HBSS and stained with the respective antibodies for 1 h. Subsequently, samples were flow sorted and cultured in alpha-minimum essential medium (MEM) (20 % fetal calf serum (FCS), 1 % penicillin/streptomycin, 1 % L- glutamine).

2.7. Immunofluorescence staining

30,000 MSC were plated on round 15 mm diameter coverslips for at least 24 h. Cells were then washed with PBS and subsequently fixed in 4 % paraformaldehyde (Cat. No. CAS 50–00-0, Santa Cruz Biotechnology, Dallas, Texas, United States) for 10 min at room temperature. Paraformaldehyde-fixed cells were permeabilized with 0.25 % Triton in PBS for 3 min. Prior to incubation with primary antibodies, cells were blocked in 2 % BSA in PBS for 2 h at room temperature. Cells were then stained overnight with phalloidin primary antibody (Table 1). The next day, the cells were washed twice with PBS and the nuclei were counterstained with 5 μg/mL DAPI (D9542, Merck, Darmstadt, Germany). Cells were washed in PBS and briefly in water and mounted with FluorMount plus 50 μg/mL DABCO (Cat. No. D27802, Sigma-Aldrich, Munich, Germany). Specimens were analyzed using a confocal laser scanning microscope (Leica SP5, Wetzlar, Germany) and pictures were

quantified using ImageJ.

2.8. Adipocyte and osteoblastic differentiation of MSC

For the differentiation assays MSC were plated in a 48-well plate (10^4 cells per well). Osteoblastic differentiation was initiated, when the cells reached a confluence of 60 %, while adipogenic differentiation was initiated at a confluence of approximately 90 %. MSC were differentiated into osteoblastic cells for approximately 10 days using osteogenic medium (α- MEM containing 20 % fetal bovine serum (FBS), 1 % penicillin/streptomycin and 1 % L-glutamine supplemented with 50 μg/mL ascorbic acid (Cat. no. A5960, Sigma-Aldrich, Darmstadt, Germany), 10 mM β-glycerophosphate (Cat. no. G9422, Sigma-Aldrich, Darmstadt, Germany) and 10 mM dexamethasone (Cat. no. 50022, Merck, Darmstadt, Germany). To test osteoblastic differentiation, cells were stained with alizarin red S (Cat. No. TMS-008, Sigma-Aldrich, Darmstadt, Germany) solution after 10–14 days of culture. Briefly, cells were fixed using 4 % paraformaldehyde (Cat. No. CAS30525–89-4, Santa Cruz Biotechnology, Dallas, Texas, United States), and subsequently washed and stained with alizarin red S stain. The cells were thoroughly washed with water before pictures were acquired.

Adipogenic differentiation was performed using commercially available differentiation and maintenance medium (Cat. no. PT3102A, PT3102B, Lonza, Cologne, Germany).

Staining of adipocytes was performed using Oil Red O dye (Cat. No. 1.02419, Sigma-Aldrich, Darmstadt, Germany). Briefly, cells were fixed using 4 % paraformaldehyde (Cat. No. CAS30525–89-4, Santa Cruz Biotechnology, Dallas, Texas, United States) and subsequently washed and stained with Oil Red O. The cells were thoroughly washed with water before pictures were acquired.

2.9. Colony forming units – fibroblast (CFU-F)

CFU-F assays were performed by seeding 10^3 MSC in a 6 cm dish. MSC culture medium was used for maintenance and was changed every 5 days. Two weeks after seeding the colonies were enumerated following staining with crystal violet dye (Cat. no. V5265, Sigma-Aldrich, Darmstadt, Germany).

Crystal violet staining was performed after fixing the cells with paraformaldehyde. The cells were washed twice with PBS, before the crystal violet stain (Cat. No. HT901 – 8FOZ, Sigma-Aldrich, Darmstadt, Germany) was added. The slides were stained for 20 min at room temperature. Subsequently, the slides were washed twice with PBS, the plates were dried and the colonies were counted.

2.10. Colony-forming unit (CFU) assays for hematopoietic cells

Colony forming unit assays for hematopoietic cells were performed in methylcellulose (MethoCult™ GF M3434, STEMCELL Technologies, Vancouver, Canada) following the manufacturer's instructions. Briefly, cells were collected from the total bone marrow of WT or SPOCK2 KO mice. The cells were ACK (ammonium-chloride-potassium) lysed (Cat. No. A1049201, Thermo Fisher Scientific, Waltham, MA, United States) and enumerated. We plated 10^4 cells per plate in duplicate, and colonies were counted 7 days after plating.

2.11. Colony forming unit – osteoblasts (CFU-Ob) and alkaline phosphatase (ALP) staining

Bone marrow was flushed, and total bone marrow cells were resuspended in complete α-MEM medium at a final density of 10^6 cells/mL. A total of 2 mL of the cell suspension was plated into each well of a 6-well culture plate. To induce osteoblast colony formation, mineralization medium containing 50 μg/mL L-ascorbic acid (AA) and 10 mM β-glycerophosphate (β-GP) was added. Working concentrations were prepared fresh for each medium change by diluting the stocks into complete α-MEM, followed by sterile filtration. The culture medium was replaced three times per week for two weeks. After the induction period, cells were fixed and stained for alkaline phosphatase (ALP) activity. Colonies with a diameter >2 mm were counted and recorded as CFU-Ob.

Cells were fixed using 3.7 % paraformaldehyde (PFA) for 20–30 min at room temperature. Following fixation, cells were washed with phosphate-buffered saline (PBS) prior to staining. The ALP staining solution was prepared as follows: 5 mg of naphtol AS-MX phosphate (Sigma, N-4875, St Louis, MO) was first dissolved in 0.25 mL of *N*,*N*-dimethylformamide. To this, 50 mL of 0.1 M Tris buffer (pH 8.5) was added, followed by the addition of 30 mg of Fast Blue BB salt (Sigma, F-0250, St Louis, MO). ALP stain was then added for 45 min at room temperature in the dark. Cells were subsequently washed three times with PBS, and colonies were then quantified.

2.12. Enzyme-linked immunosorbent assay (ELISA)

The samples for ELISA were collected by flushing the femora of WT or SPOCK2 KO mice using PBS (300 μl). This was followed by centrifugation at 1200 rpm. The supernatant was collected and stored at −80 °C until the assay was performed. ELISA for C-telopeptide of type I collagen (CTX—I, Cat. no.: MBS703094, Mybiosource.inc. Vancouver, Canada) and procollagen I N-terminal propeptide (PINP, Cat. no. MBS2500076, Mybiosource.inc. Vancouver, Canada) were performed following the manufacturer's instructions.

2.13. Seahorse metabolic flux analysis

The cellular oxygen consumption rate (OCR) and the extracellular acidification rate (ECAR) were analyzed using a Seahorse XFe96 extracellular flux analyzer (Agilent, Santa Clara, USA). WT and SPOCK KO MSC (10,000 cells/ well) were plated on a Seahorse 96-well cell culture plate two days prior to measurement and equilibrated for 45 min before measurement in MSC medium. Data were analyzed using Wave desktop, Microsoft Excel, and Graph Pad Prism.

2.14. Microcomputed tomography (microCT)

Assessment of bone morphology and microarchitecture of SPOCK2 KO and C57/BL6 mice was performed using micro-computed tomography (μCT40, Scanco Medical, Brüttisellen, Switzerland). Briefly, the right femora were isolated, freed of muscle and soft tissue and scanned (10μm^3 voxel size, 70 kVp peak potential, 113 μA current, and 200 msec integration time) to assess both trabecular and cortical bone microarchitecture. Trabecular bone was analyzed in a 1.5 mm long region of the distal metaphysis, segmented with a threshold of 400 mgHA/cm^3, beginning 200 μm above the growth plate and extending proximally. The analysis was performed in the Scanco Evaluation program to measure trabecular bone volume fraction (Tb.BV/TV, %), bone mineral density (Tb.BMD, mgHA/cm^3), trabecular thickness (Tb.Th, μm), trabecular number (Tb.N, mm^{-1}), trabecular separation (Tb.Sp, μm) and connectivity density (Conn.D, mm^{-3}). The cortical region was assessed in a 0.5 mm long region of the mid-diaphysis of the femur, with outcomes including cortical thickness (Ct.Th, μm), cortical tissue mineral density (Ct.TMD, mgHA/cm^3), bone area fraction (bone area (Ct.Ar)/ total area (Tt.Ar, %)) and polar moment of inertia (pMOI, mm^4).

2.15. Histological analysis

2.15.1. H&E staining

Femora were collected from mice after sacrifice and fixed in 10 % formalin at room temperature. Decalcification of bone was performed by placing the bones in 0.5 M EDTA solution at 37 degrees. After decalcification for 3 weeks the bones were mounted in paraffin and sectioned. Immunohistochemistry or H&E staining of bone sections from mice was performed following standard procedures.

2.16. CellTiter-Glo® assay for ATP measurement

The CellTiter-Glo® 2.0 Reagent (Promega: G9241, Madison, WI) was used for the comparison of ATP production by WT versus SPOCK2 KO MSC. The MSC were seeded into opaque-walled, white multi-well plates at optimized densities in complete culture medium. Ten thousand cells were cultured (96 well plate) under standard culture conditions (37 °C, 5 % CO_2) in complete MEM-α medium. For background controls, wells containing medium without cells were prepared. Twenty-four hours later the cells were used for ATP measurement. CellTiter-Glo® 2.0 reagent was equilibrated to room temperature for approximately 30 min. An equal volume of CellTiter-Glo® 2.0 reagent was added to each well (e.g., 100 μL reagent to 100 μL medium in a 96-well plate). The plate was then shaken on an orbital shaker for 2 min to induce cell lysis. Following mixing, the plate was incubated at room temperature to allow luminescent signal stabilization, according to the manufacturer's instructions. Luminescence was measured using a compatible microplate luminometer. Background signal from control wells (medium only) was subtracted from experimental readings.

2.17. Immunoblotting

RIPA buffer (50 mM Tris HCl pH 7.4, 150 mM NaCl, 1 % Triton X-100, 1 % Na DOC, 0.1 % SDS, 1 mM EDTA) was used to lyse primary samples or cultured cells. It was freshy supplemented with protease and phosphatase inhibitor cocktails (Cat. No. 04693159001, Sigma-Aldrich, Darmstadt, Germany). The lysates were kept on ice for 20 min followed by centrifugation (4 °C for 20 min at 14000 rpm). The Bradford protein assay (Bio-Rad, Hercules, CA, USA) was used to quantify the proteins. Quantified protein was denatured using 4× Laemmli buffer, supplemented with β-mercaptoethanol, and denatured at 95 °C for 5 min. The samples were then run on 4–12 % Bis-Tris polyacrylamide gels (Cat. No. NP0321BOX, ThermoFisher Scientific, Darmstadt, Germany). The proteins were blotted on PVDF membranes (Cat. No. 88518, ThermoFisher Scientific, Darmstadt, Germany), and overnight staining with the respective antibodies (1:500 dilution) at 4 °C was then performed. On the following day the secondary antibody was added for 2 h at room temperature and the blots were subsequently developed.

2.18. Statistics

GraphPad (Prism 8.0 and higher) was used for all statistical analyses. For every experiment, there were three to eight distinct biological replicates. In case of normal distribution, a two-tailed *t*-test was used, when the means of two groups were being compared. When multiple hypotheses were tested, one-way or two-way ANOVA and Tukey or Sidak tests (the latter for multiple comparisons) were used as post-hoc tests. *P* values <0.05 were regarded as significant. The data were shown as mean ± s.d.

3. Results

3.1. Generation of SPOCK2 KO mice

Initially, we tested expression of SPOCK2 protein in different murine tissues. Western blot analysis confirmed the variability in expression of SPOCK2 in different tissues, with higher expression of SPOCK2 being found in spleen, liver and bone marrow (Fig. 1A). As these three tissues in the murine system are involved in (extramedullary) hematopoiesis, we investigated the role of SPOCK2 in hematopoiesis and skeletal homeostasis. To test this, we generated SPOCK2 knockout (KO) mice by CRISPR-CAS in a C57BL/6NTac background (Fig. 1B, Supplementary figs. 1A-C). The mice were bred as both heterozygous x heterozygous (HETxHET) and homozygous x homozygous (HOMxHOM), but only homozygous KO mice were used in our experiments. The loss of SPOCK2 in mesenchymal stromal cells (MSC) (Fig. 1C), an important population of the BMM, and lineage-negative (Lin-) ($CD5^-$ (T cells), $B220^-$ (B cells), $Gr\text{-}1^-$ (myeloid cells), F4/80 (macrophages), $Ter119^-$ (erythroid cells)) hematopoietic cells (Fig. 1D) in wildtype (WT) versus SPOCK2 KO mice was confirmed using Western blotting. In WT mice, SPOCK2 is expressed in Lin- cells and MSC, but not in adipocytes, differentiated from MSC (Fig. 1E). Taken together, SPOCK2 expression is highest in hematopoietic tissues, and SPOCK2 KO mice, which are viable and fertile, were successfully generated.

3.2. SPOCK2 deficiency leads to differences in bone density and mineralization

To test, if the loss of SPOCK2 leads to alterations in bone architecture and mineralization, we performed a microCT analysis of femora from 10 to 14 week-old female WT vs SPOCK2 KO mice (Fig. 2A). This revealed a significant decrease in trabecular bone volume over total tissue volume (BV/TV %) ($P = 0.0007$; Figs. 2B), trabecular bone mineral density (BMD) (Tb. BMD) ($P = 0.0035$; Fig. 2C), trabecular thickness (Tb. Th ($P = 0.0378$; Fig. 2D), and connectivity density (ConnD ($P = 0.0405$); Fig. 2E) in bones from SPOCK2 KO compared to WT mice. Other parameters such as trabecular number (Tb.N) (Fig. 2F) or trabecular separation (Tb.Sp) (Fig. 2G) showed no differences between SPOCK2 KO and WT bones. The cortical area, as assessed by analysis of the femur midshaft, showed a significant increase in total mineral density (Ct. TMD) in SPOCK2 KO compared to WT bones ($P = 0.0015$; Figs. 2H-I). Cortical area (Ct.Ar) (Fig. 2J), medullary (or marrow) area (Ma.Ar) (Fig. 2K), cortical porosity (Fig. 2L) or cortical bone area fraction (CtAr/TtAr) (Fig. 2M) did not differ between SPOCK2 KO and WT bones. Taken together, these results suggest that, in female mice, SPOCK2 exerts opposite effects in the two bone compartments. In the absence of SPOCK2 there is trabecular bone loss which is associated with an increase in cortical mineral density.

3.3. Osteoclast number and bone resorption is increased in trabecular bone of SPOCK2 KO mice

To investigate the cellular mechanisms driving trabecular bone loss, we analyzed osteoclast number and activity in the bone marrow, by performing tartrate-resistant acid phosphatase (TRAP) staining of bone sections and found a significant increase in the number of $TRAP^+$ cells in bones isolated from SPOCK2 KO compared to WT mice ($P < 0.0001$; Figs. 3A-B). In addition, the ratio of the number of TRAP+ osteoclasts to the bone surface ($P = 0.0064$; Fig. 3C) and the ratio of the osteoclast surface to bone surface ($P = 0.0138$; Fig. 3D) were significantly higher in SPOCK2 KO mice. In enzyme-linked immunosorbent assays to detect the amount of C-terminal telopeptide of type I collagen (CTX) (to test bone resorption) and procollagen type I N-propeptide (P1NP) (to test bone formation) in the bone marrow supernatant of bones from WT or SPOCK2 KO mice we found, that, compared to WT mice, there was a significant increase in the amount of CTX-1 in the BM of female ($P = 0.0182$; Fig. 3E), but not male (Supplementary fig. 2 A) SPOCK2 KO mice. No differences were observed in the serum level of CTX-1 (Supplementary fig. 2B). Similarly, the ratio of RANKL/OPG (receptor activator of NF-κB ligand / osteoprotegerin) was unchanged in the mRNA from flushed SPOCK2 KO bones, compared to WT (Fig. 3F). Assessing osteoblasts, we found that expression of *Bglap* (bone γ-carboxyglutamate protein; osteocalcin) was increased in mRNA isolated from flushed and crushed bones of SPOCK2 KO mice (Fig. 3G, Table 2), but P1NP did not show any differences (Supplementary fig. 2C). Taken together, these data suggest that in the absence of SPOCK2 expression there is a significant decrease in trabecular bone and bone density, likely driven by increased bone resorption in female mice, as suggested by the increase in osteoclasts in SPOCK2-deficient bones. In contrast, the cortical compartment is slightly increased, as demonstrated by a significant increase in cortical mineral density, which is also associated with an increase in osteocalcin mRNA expression.

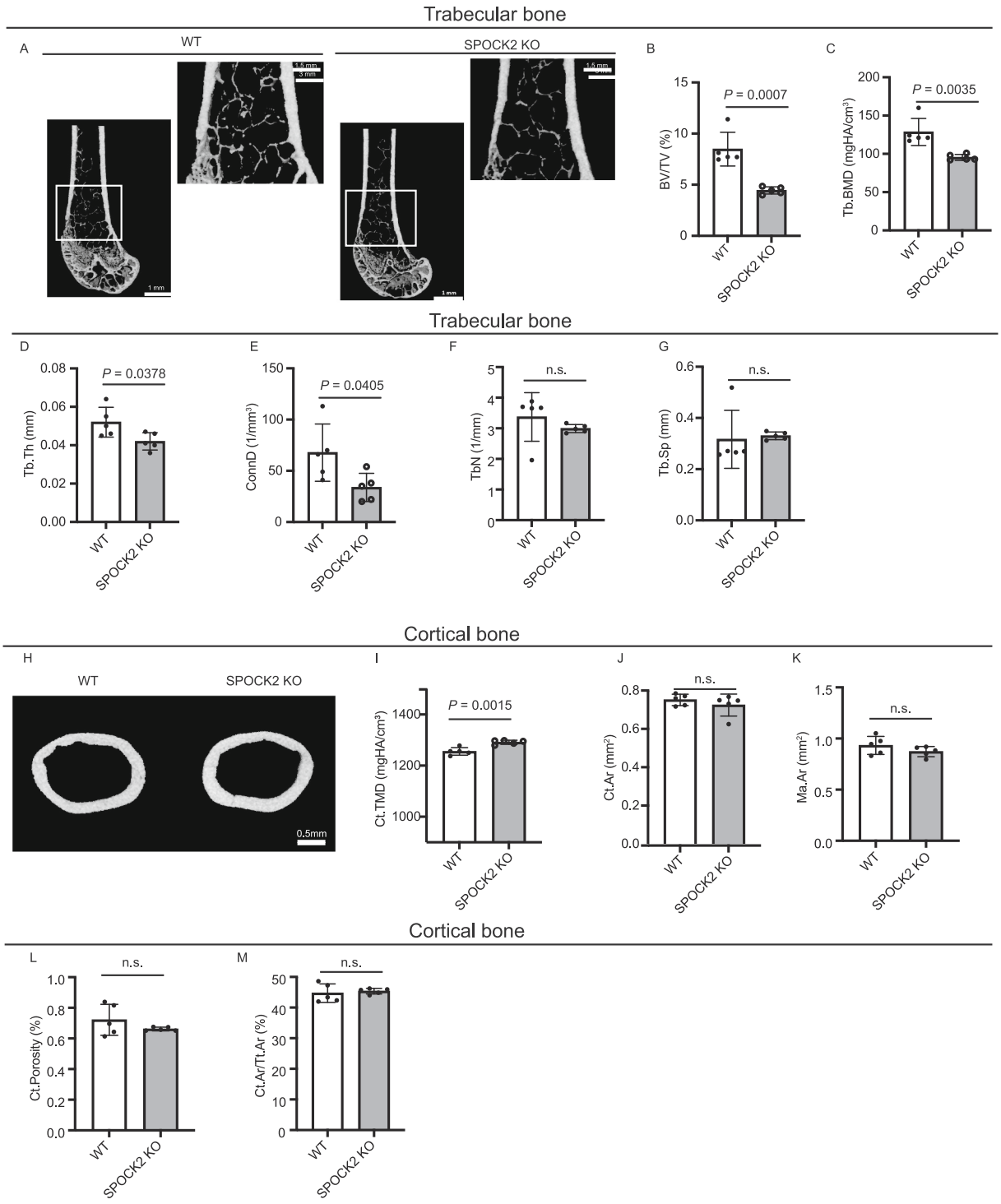

Fig. 2. A) Representative images of longitudinal sections with their respective magnified (3x) images as insets of femoral bones from WT versus SPOCK2 KO mice, as visualized by μCT analysis. B-G) Percentage of trabecular bone volume of total bone volume (BV/TV (bone volume/total volume) in percent (B) ($P = 0.0007$, *t*-test, $n = 5$), trabecular bone mineral density/cm^3 (C) (BMD) (Tb.BMD) ($P = 0.0035$, t-test, n = 5), trabecular thickness in mm (D) (Tb.Th ($P = 0.0378$, *t*-test, n = 5), connectivity density/mm^3 (E) (ConnD ($P = 0.0405$, t-test, n = 5), trabecular bone number (TbN) per mm (n = 5) (F), trabecular bone separation (G) (Tb.Sp) (n = 5), quantified by μCT in bones from WT or SPOCK2 KO mice. H) Representative images (cross section) of femoral bones of WT versus SPOCK2 KO mice, as visualized by μCT analysis. I-M) Cortical bone mineral density (I) (Ct.Total mineral density/cm^3 (TMD) $P = 0.0015$, t-test, n = 5), cortical area (Ct.Ar/mm^2) (J), medullary area (Ma.Ar/mm^2) (K), cortical porosity in percent (L), and the ratio of the cortical area of the total area in percent (Ct.Ar/Tt.Ar) (M) in bones from WT versus SPOCK2 KO mice, as visualized by μCT analysis (n = 5).

3.4. Mesenchymal stromal cells from SPOCK2 KO mice show altered morphology and differentiation capacity

MSC are important constituents of the BMM, as they differentiate into chondrocytes, adipocytes and osteoblasts [27]. As MSC are known to control hematopoietic stem and progenitor cells (HSPC) [2], we investigated whether these cells were affected by the absence of SPOCK2. Indeed, MSC were significantly decreased in SPOCK2 KO

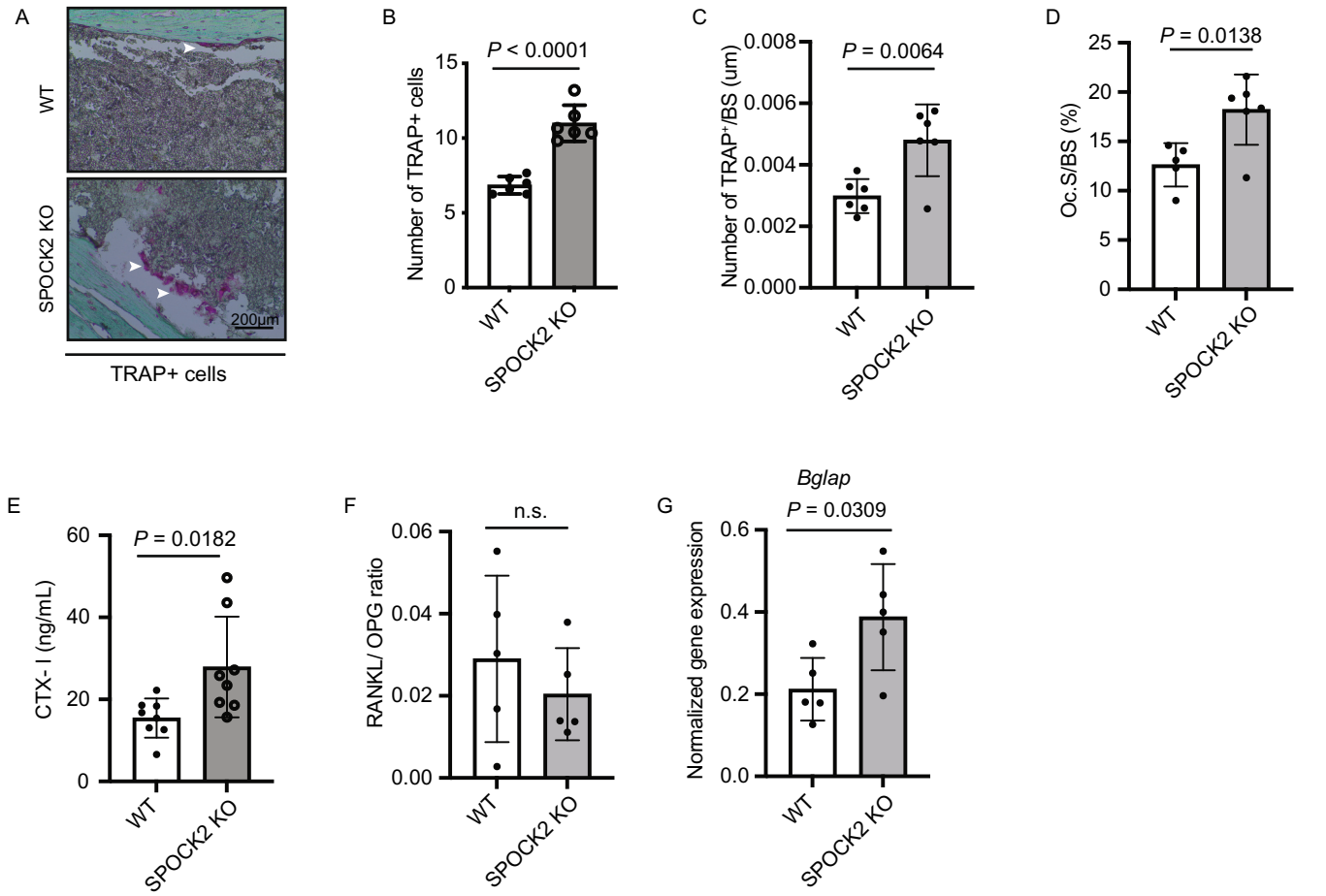

Fig. 3. A-B) Representative image of TRAP staining in bone sections of WT or SPOCK2 KO mice. TRAP positive cells are purple and indicated by white arrowheads. The scale bar represents 200 µm (A). The number of TRAP$^+$ cells in bone sections of WT or SPOCK2 KO mice is shown in (B) ($P < 0.0001$, t-test, $n = 6$). C—D) Number of TRAP+ cells (osteoclasts) per bone surface (Oc.N/BS; cells/ µm) (C) ($P = 0.0064$, *t*-test, n = 6) and ratio of osteoclast surface to bone surface (Oc.S/BS in %) (D) ($P = 0.0138$, *t*-test, n = 6) in bone sections of WT or SPOCK2 KO mice. The quantifications were performed with ImageJ. E) Levels of C-terminal telopeptide of type I collagen (CTX-1) in the bone marrow supernatant of female WT versus SPOCK2 mice, measured by ELISA ($P = 0.0182$, *t*-test, $n = 8$). F) Ratio of RANKL (Receptor Activator of NF-κB Ligand)/ OPG (Osteoprotegerin) (*Tnfsf11/ Tnfrsf11b*), as measured by qPCR of RANKL (*Tnfsf11*) and OPG (*Tnfrsf11b*) in flushed and subsequently crushed bone from WT or SPOCK2 KO mice (n = 5). G) Gene expression of *Bglap* (Bone γ-carboxyglutamate protein; osteocalcin) ($P = 0.0309$, *t*-test, n = 5) in flushed and crushed bones of WT or SPOCK2 KO mice, normalized to *Gapdh* (Glyceraldehyde 3-phosphate dehydrogenase). (For interpretation of the references to colour in this figure legend, the reader is referred to the web version of this article.)

compared to WT mice ($P = 0.0354$, Fig. 4A). Furthermore, colony-forming fibroblast (CFU-F) ability of SPOCK2 KO MSC was significantly reduced compared to WT MSC from female and male mice ($P = 0.0388$, Figs. 4B-C, Supplementary fig. 3 A). Additionally, the morphology and size of MSC derived from female and male SPOCK2 KO mice differed significantly from WT MSC, as SPOCK2 KO MSC were significantly smaller ($P < 0.0001$, Figs. 4D-E, Supplementary figs. 3B—C). Testing the differentiation ability of MSC, we observed that MSC derived from SPOCK2 KO mice had reduced propensity to differentiate into adipocytes ($P = 0.0144$, Figs. 4F-G), as demonstrated by a reduced number of oil-red positive adipocytes and reduced expression of the adipocyte-associates genes *Adipoq* (adiponectin) ($P = 0.0097$, Fig. 4H) and *Plin5* (perilipin) ($P = 0.0194$, Figs. 4I) in MSC differentiated into adipocytes from SPOCK2 KO compared to WT mice. *Pparg* (Peroxisome Proliferator Activated Receptor Gamma; PPAR γ) expression was reduced, although this did not reach significance ($P = 0.0698$, Fig. 4J). H&E staining of bone sections also revealed a reduction in the overall number of adipocytes ($P = 0.0143$, Figs. 4K-L), but no difference was found in the inguinal or perirenal fat mass between WT and SPOCK2 KO mice (Supplementary figs. 3D-E). Expression of *Adipoq, Plin5* and *Pparg* also did not differ in inguinal or perirenal fat tissue in WT or SPOCK2 KO mice (Supplementary figs. 3F—K).

MSC from SPOCK2 KO mice demonstrated higher osteogenic differentiation than their WT counterparts, as shown by increased colony-forming units osteoblasts (CFU-Ob) ($P = 0.0341$, Figs. 4M-N) and increased alizarin red staining ($P < 0.0001$, Figs. 4O-P).

Consistently, gene expression analysis of MSC from SPOCK2 KO versus WT mice revealed significant alterations in pathways associated with stemness, inflammation and cell migration (Fig. 4Q, Supplementary fig. 4 A). Reactive oxygen species, DNA damage and metabolic activity (extracellular acidification rate (ECAR), oxygen consumption rate (OCR), ATP-coupled respiration, maximal respiration and levels of ATP in MSC from SPOCK2 KO versus WT mice did not differ significantly (Supplementary figs. 4B—H). In summary, in mice lacking SPOCK2 MSC are decreased in number, and they demonstrate altered differentiation capacity and an inflammatory genetic signature. Importantly, in the absence of SPOCK2, the osteogenic differentiation of MSC is increased, whereas adipogenic differentiation is reduced. The increase in CFU-Ob present in SPOCK2 KO mice can partially explain the increased cortical bone mineral density (Fig. 2I) and the increased osteocalcin gene expression (Fig. 3G) present in these mice.

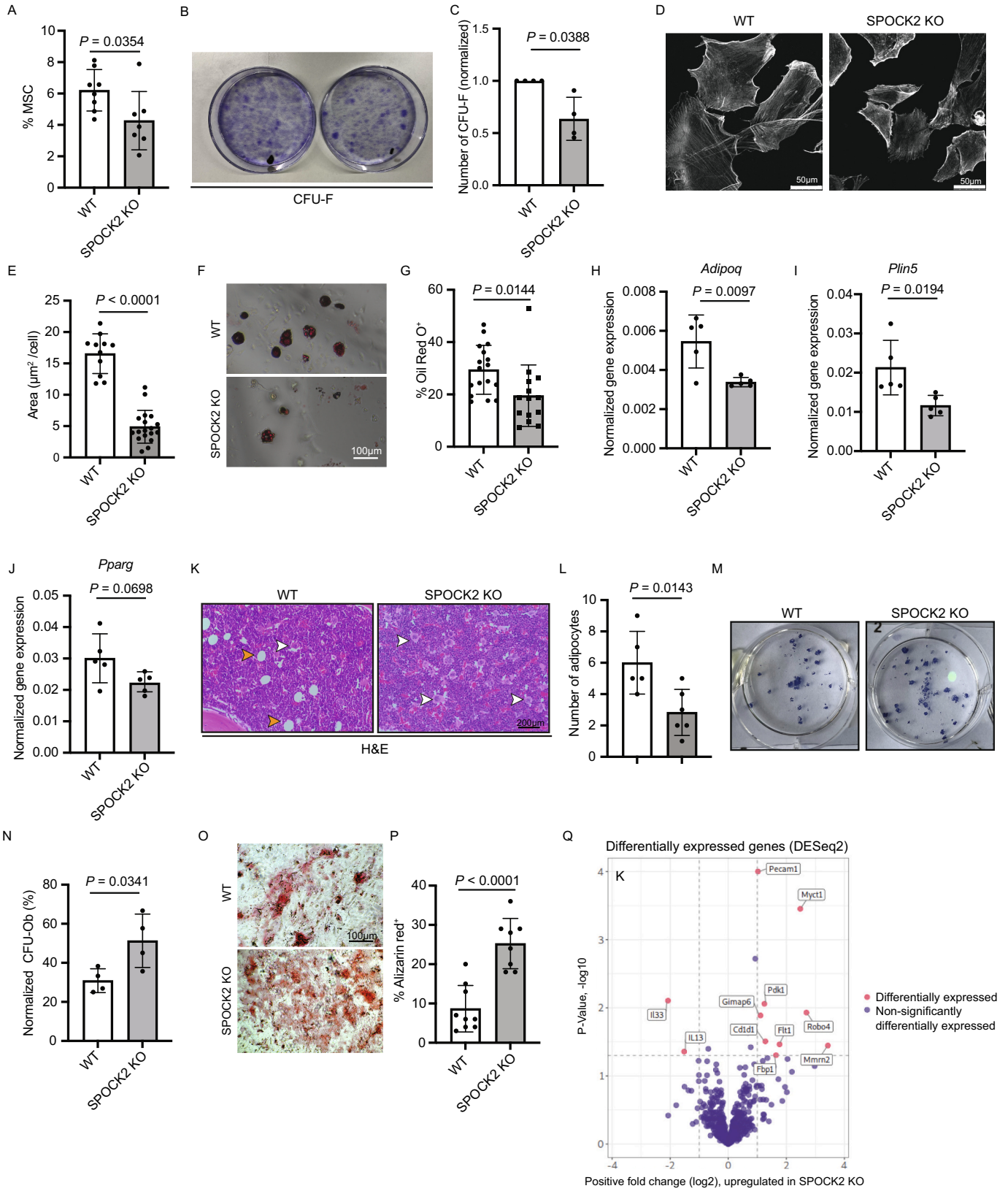

(caption on next page)

Fig. 4. A) Percentage of MSC (PDGFRα$^+$, Sca1$^+$, CD45$^-$, Ter119$^-$) of all cells in the bone marrow of WT versus SPOCK2 KO mice ($P = 0.0354$, *t*-test, $n = 7$–8). B—C) Representative image of colony forming units - fibroblast (CFU-F) (B) and number of colonies (normalized to WT mice) using WT versus SPOCK2 KO MSC ($P = 0.0388$, t-test, $n = 4$). The assay was performed by culturing 10^3 MSC (WT vs SPOCK2 KO) in a 3 cm dish for two weeks in complete MSC medium, leading to the formation of fibroblastic colonies by MSC. D-E) Representative image (D) and average size in μm^2 (E) of MSC from WT versus SPOCK2 KO MSC ($P < 0.0001$, t-test). For quantification, four biological replicates of MSC were used per group and multiple [3–6] images per replicate (technical replicates) were included in the analysis. Each dot represents the average area of the cells in each image (technical replicate). F-G) Representative images (F) and quantification (G) of oil O red-positive staining performed on adipocytes differentiated from WT versus SPOCK2 KO MSC ($P = 0.0144$, t-test). For quantification, three biological replicates were used per group and multiple [3–7] images per mouse (technical replicates) were included in the analysis. Each dot represents the average percentage of positively stained colonies of adipocytes in each image (technical replicates) of all colonies. H-J) Gene expression of *Adipoq* (H) ($P = 0.0097$, t-test, n = 5), *Plin5* (I) ($P = 0.0194$, t-test, n = 5) and *Pparg* (J) ($P = 0.0698$, t-test, n = 5) in WT or SPOCK2 KO MSC, which had been differentiated into adipocytes. Gene expression, as measured by qPCR, was normalized to *Gapdh* (Glyceraldehyde 3-phosphate dehydrogenase). K-L) Representative images (K), and number of adipocytes (L) ($P = 0.0143$, t-test, n = 5–6) visualized in the field of view of hematoxylin and eosin (H&E) stained sections of bones of WT versus SPOCK2 KO mice. M-N) Representative images of colony forming unit- osteoblast (CFU-Ob) (M) and number of colonies (N) (normalized to total crystal violet+ colonies) ($P = 0.0341$, t-test, n = 4). O—P) Representative images of alizarin red staining (O) and its quantification (P) performed on osteoblastic cells differentiated from WT versus SPOCK2 KO MSC ($P < 0.0001$, t-test). For quantification of differentiation, three biological replicates were used per group and multiple [3–7] images per mouse (technical replicates) were included in the analysis. Each dot represents the average percentage of positively stained osteoblastic cells in each image (technical replicates) of all colonies. Q) Volcano plot displaying the differences in fold change (log2FC) of mRNA expression between WT and SPOCK2 KO bone marrow-derived MSC. The x-axis shows differences in log2FC, and the y-axis indicates the -log10 *p*-value. The dashed lines represent the thresholds for differential gene expression (horizontal for probability of differential expression $p < 0.05$; vertical for absolute logarithmic fold change >0.5). DE = Differentially expressed; Not-DE = Non-significantly differentially expressed. (For interpretation of the references to colour in this figure legend, the reader is referred to the web version of this article.)

3.5. SPOCK2 KO mice differ from WT mice with regards to hematopoietic stem and progenitor cells

To examine any alterations in the hematopoietic compartment, we performed a hematological analysis of peripheral blood, bone marrow and spleen from SPOCK2 KO versus WT mice. While no differences were observed in peripheral blood with regards to white blood cells (WBC), red blood cells (RBC) and hemoglobin (Figs. 5A-C), a significant reduction in the number of platelets was observed in SPOCK2 KO mice ($P = 0.0245$, Fig. 5D), although we found an increase of megakaryocytes in the femora of SPOCK2 KO mice ($P = 0.0006$, Figs. 4K, 5E). Levels of thrombopoietin, however, were similar in WT versus SPOCK2 KO mice (Supplementary fig. 5A). Myeloid cells (CD11b$^+$), T cells (CD5$^+$), B cells (B220$^+$) and erythroid precursors (Ter119$^+$) in peripheral blood, bone marrow and spleen did not differ between WT and SPOCK2 KO mice (Supplementary figs. 5B—D). As the ECM and specifically SPARC have been associated with alterations of B cell number [28,29], we tested B cell subsets, but these did not differ between both cohorts (Supplementary fig. 5E). Additionally, no differences were found between common myeloid progenitors (CMP), granulocyte monocyte progenitors (GMP), megakaryocyte- erythrocyte progenitors (MEP) and multipotent progenitors (MPP) in bone marrow or spleen of SPOCK2 KO compared to WT mice (Supplementary figs. 5F-G). Common lymphoid progenitors (CLP) were significantly increased in the BM, but not the spleen of SPOCK2 KO compared to WT mice ($P = 0.0387$, Supplementary figs. 5H—I). We found trends towards a reduction of myeloid-biased MPP2 (Fig. 5F) and CD41$^+$ cells (myeloid-biased long-term HSC) (Fig. 5G). Additionally, a significant increase of the number (normalized) ($P = 0.0262$, Fig. 5H) and a strong trend towards an increase in the percentage of LKS per femur (normalized) ($P = 0.056$, Fig. 5I) were observed for Lin$^-$ c-Kit$^+$ Sca1$^+$ (LKS) cells in the bone marrow of SPOCK2 KO compared to WT mice. The number of LKS cells in the spleen did not differ (Supplementary fig. 5J). A colony-forming unit (CFU) assay revealed an increase in colony-forming ability of total bone marrow (hematopoetic) cells derived from SPOCK2 KO mice (Figs. 5J-K). We next performed differential gene expression analysis to compare the gene expression profiles of LKS cells derived from WT or SPOCK2 KO bone marrow. We identified 29 significantly differentially expressed genes, amongst which we identified genes associated with inflammation, chemotaxis, differentiation and migration (Fig. 6A). Gene set enrichment analysis of differential gene expression results also suggested a downregulation of targets/genes associated with inflammation and TNF signaling pathways (Figs. 6B-C, Supplementary fig. 6A) and upregulation of genes involved in interferon signaling, lymphocyte and B cell activation pathways (Figs. 6D-F) in LKS cells from SPOCK2 KO compared to WT mice. Taken together, LKS cells may be increased in the bone marrow of SPOCK2 KO mice, possibly due to increased interferon signaling, and may reveal a gene signature associated with altered inflammation and chemotactic activity. The increase in lymphocyte activation pathways may underlie the increase in CLP in the bone marrow.

4. Discussion

MSC represent an important population of the BMM, influencing HSC maintenance and function [2,30–32], as well as controlling skeletal homeostasis by differentiating into osteoblasts and other cells. However, the question of how MSC themselves are regulated has not been sufficiently addressed. Different components of the ECM like fibronectin, collagen, hyaluronan and others are known to interact with membrane receptors of MSC, determining their differentiation and function [33].

In the current manuscript, we have identified SPOCK2 as a regulator of MSC number, phenotype and function. Our data suggest that loss of SPOCK2 alters MSC phenotype, lineage commitment, as well as colony-forming ability. Loss of SPOCK2 favors osteogenic differentiation of MSC while reducing the number of adipogenic progenitors, as shown by significant changes in CFU-Ob, increased osteocalcin expression, reduced adipocytic differentiation of SPOCK2 KO MSC and reduced adipocytes in the bone marrow of SPOCK2 KO mice. Interestingly, the increase in osteoprogenitors is associated with an increase in cortical mineral density and a decrease in trabecular bone volume, suggesting that the different skeletal compartments are differentially regulated by SPOCK2. Indeed, the increase in CFU-Ob is linked with an increase in osteocalcin mRNA expression, partially explaining the increased cortical density. On the other hand, SPOCK2 mice also develop trabecular bone loss driven by increased osteoclast number and activity. Further studies will be needed to delineate the molecular mechanisms involved.

Other studies have suggested that in vitro maintenance [34] or differentiation of MSC into different lineages is dependent on the presence of the ECM [35,36]. For example, interaction of integrins (α2β1 and α11β1) on human MSC with collagen I promotes MSC survival, as well as osteogenic differentiation [37]. Similarly, activation of integrin α5 signaling led to activation of the focal adhesion kinase (FAK)-ERK1/2-dependent pathway and osteogenic differentiation of human BM MSC [38]. Furthermore, our nanostring data reveal significant alterations in expression of genes involved in stemness and inflammation in SPOCK2 KO versus WT MSC.

Our microCT analysis of bone revealed that deficiency of SPOCK2 has a profound effect on trabecular bone, with decreased trabecular bone mineral density and thickness, whereas cortical bone is not affected. This effect may be attributed to differential localization of SPOCK2 or SPOCK2-generating MSC, osteoblastic cells or osteoclasts in

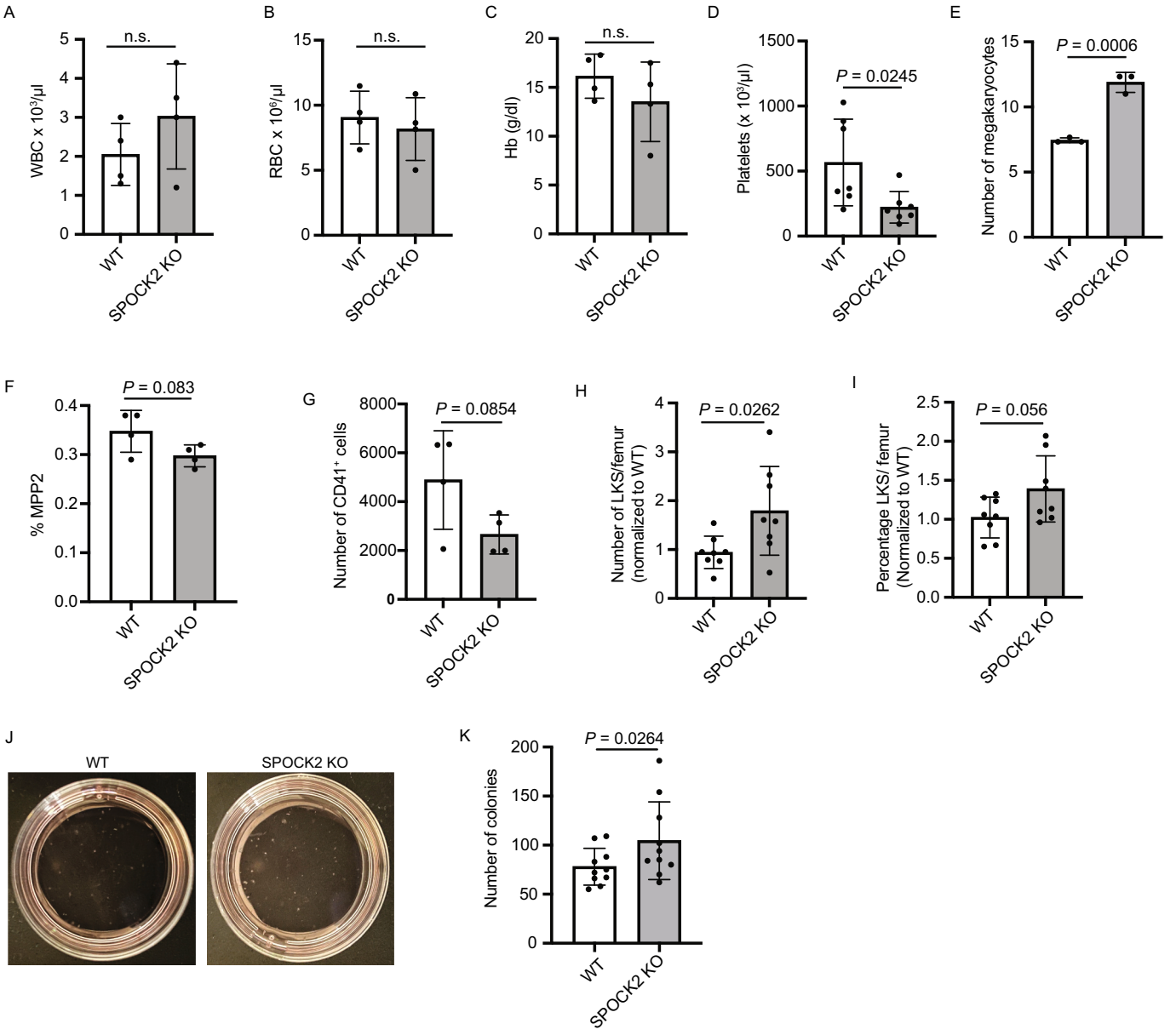

Fig. 5. A-D) Leukocyte count (x 10^3/µl) (A), red blood cell (RBC) count (x 10^6/µl) (B), hemoglobin (Hb) (g/dl) (C), and platelet count (D) (x 10^3/µl) ($P = 0.0245$, t-test, n = 4) in the peripheral blood of WT versus SPOCK2 KO mice. E) Number of megakaryocytes (E) ($P = 0.0006$, t-test, $n = 3$) visualized in the field of view of hematoxylin and eosin (H&E) stained sections of bones from WT versus SPOCK2 KO mice (as seen in Fig. 4K). F) Percentage of multipotent progenitor 2 (MMP2) cells in the bone marrow of WT versus SPOCK2 KO mice ($P = 0.083$, t-test, n = 4). G) Number of $CD41^+$ cells in the bone marrow of WT versus SPOCK2 KO mice ($P = 0.0854$, t-test, n = 4). H) Number of LKS cells (normalized to WT mice) in the bone marrow of WT versus SPOCK2 KO mice ($P = 0.0262$, t-test, $n = 8$). I) Percentage of LKS cells (normalized to WT mice) in the bone marrow of WT versus SPOCK2 KO mice ($P = 0.056$, t-test, n = 8). J-K) Representative images (J) and quantification (K) of colony-forming unit (CFU)-assays after plating of 10^4 total bone marrow (hematopoietic) cells from WT or SPOCK2 KO mice in methylcellulose ($P = 0.0264$, t-test, $n = 10$). (For interpretation of the references to colour in this figure legend, the reader is referred to the web version of this article.)

trabecular versus cortical SPOCK2 KO bone. Differential contributions of trabecular versus cortical bone to bone physiology, particularly in female versus male mice, may, therefore, nullify overall parameters of bone turnover, such as the RANKL/OPG ratio or may be due to differences between measured RNA versus protein levels. Regardless, the bone loss in female SPOCK2 KO mice is likely driven by increased bone resorption which is associated with a significant decrease in MSC number. The lack of an increase of the RANKL/OPG ratio in SPOCK2 KO mice may suggest that other contributors to osteoclastogenesis such as tumor necrosis factor (TNF)α [39,40] and/or interleukin-1β [41] may, respectively, be at stake.

Our observations that MSC progenitor cell function was reduced in SPOCK2 KO mice, but that these cells displayed increased osteogenic ability, was unexpected. But MSC-intrinsic alterations leading to reduced CFU-F formation by SPOCK2-deficient MSC or an altered composition of the ECM may explain the aberrant phenotype. In fact, the ECM is beginning to be recognized as a vital component of the BMM, regulating bone formation, as well as the function of hematopoietic cells, for example via the release of growth factors stored in the ECM, in physiological conditions, but also in the hematological malignancies [42]. Although collagen type I is a major contributor to the mineralization of bone and bone turnover, non-collagenous proteins also play a vital role in bone physiology [43]. For instance, absence of circulating fibronectin led to a reduced matrix-to-mineral ratio and altered biomechanical properties of bone in the murine system [44]. Additionally, loss of osteonectin, another SPARC family member, led to a

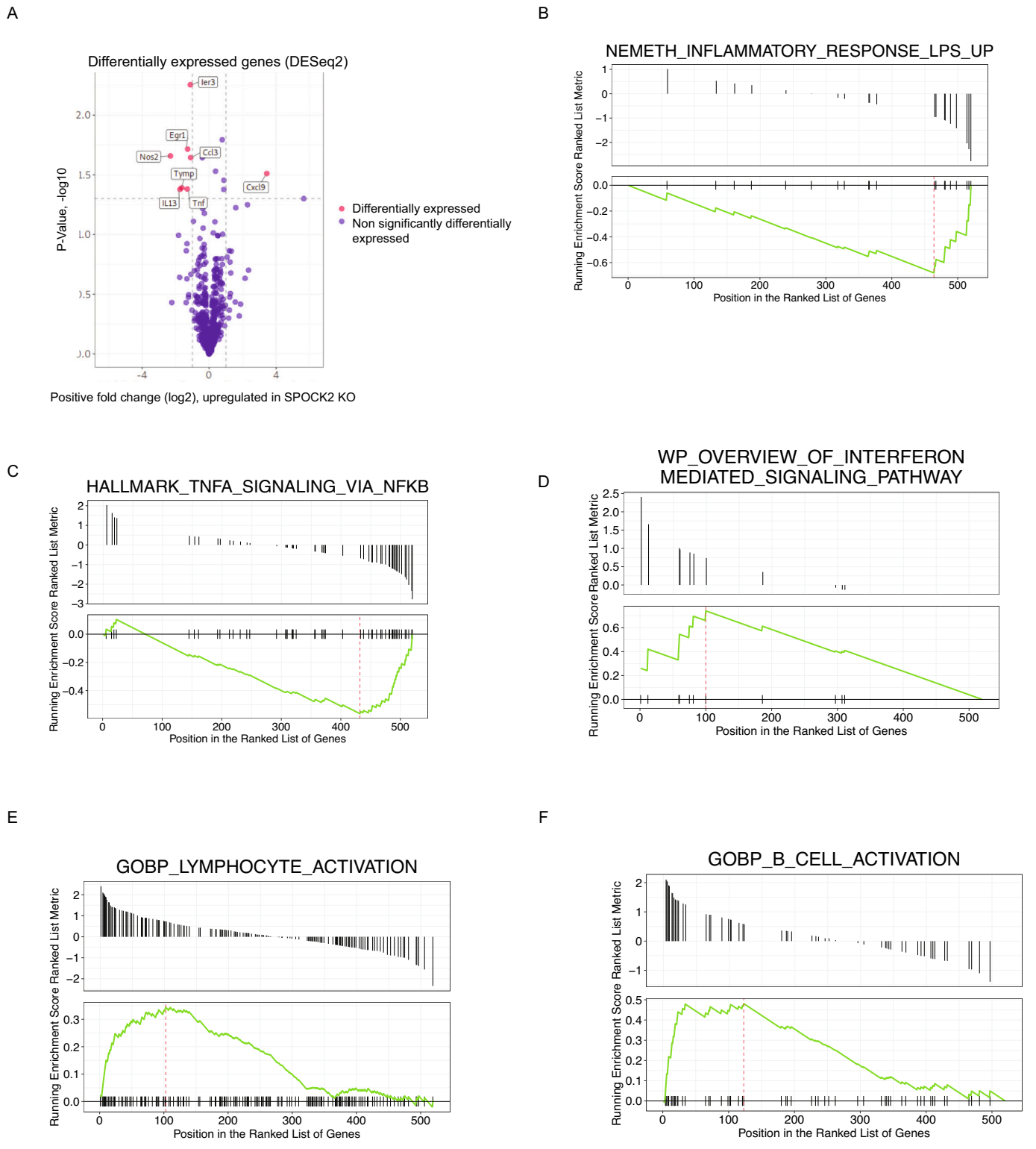

Fig. 6. A) Volcano plot displaying the logarithmic fold change (log2FC) of mRNA expression between WT and SPOCK2 KO bone marrow-derived Lin- c-Kit+ Sca1+ (LKS) cells. The x-axis shows differences in log2FC, and the y-axis indicates the -log10 p-value. The dashed lines represent the thresholds for differential gene expression (horizontal for probability of differential expression $p < 0.05$; vertical for absolute logarithmic fold change >1). (DESeq2 statistical test). B—F) Gene set enrichment analysis (GSEA) on differential gene expression results between WT and SPOCK2 KO bone marrow-derived Lin- c-Kit+ Sca1+ (LKS) cells. Genes are ranked according to differential expression statistics (x-axis). The y-axis in the top panels shows the value of the differential expression statistic (stat value) used for ranking (only genes belonging to the respective gene set are shown). The y-axis in the lower panel indicates the running enrichment score gene sets: NEMETH_INFLAMMATORY_RESPONSE_LPS_UP (B), HALLMARK_TNFA_SIGNALING_VIA_NFKB (C), WP_OVERVIEW_OF_INTERFERON MEDIATED_SIGNALING_PATHWAY (D), GOBP_LYMPHOCYTE_ACTIVATION (E) and GOBP_B_CELL_ACTIVATION (F). A positive enrichment score indicates an upregulation of genes from a given gene set in the SPOCK2 KO condition.

bone phenotype similar to that in SPOCK2 KO mice, namely osteopenia and shortened femora [45]. Deficiency of tenascin-X (TNX), another glycoprotein of the ECM, was also associated with reduced bone density and increased osteoclast activity [46]. In hematopoiesis, laminins, for example, have been shown to regulate the homing and cycling ability of hematopoietic stem and progenitor cells, and, thereby, the reconstitution of bone marrow post irradiation [47]. Similarly, laminin can regulate the adhesion and migration of hematopoietic progenitor cells [48], and fibronectin also plays a role in hematopoiesis via its binding to several receptors [49]. SPARC, a member of the same superfamily to which also SPOCK2 belongs, plays a role in HSC maintenance post 5-fluorouracil-induced stress by regulating niche function [50]. While SPARC has been shown to be dispensable for HSC number and murine hematopoiesis [51], our data, in contrast, suggest a regulation of HSC number by SPOCK2 with an increase in the number of LKS cells in bone marrow. However, the increase in megakaryocytes in the bone marrow of SPOCK2 KO mice remains unclear.

We also observed an alteration of the colony-forming ability of SPOCK2 KO hematopoietic cells, as well as an increase in the number of common lymphoid progenitors suggesting that lack of another ECM protein, SPOCK2, may lead to altered differentiation capacity of HSC. However, these differences may lie in the SPOCK2-deficient HSPC, the BMM or both, but HSC function would need to be addressed in transplantation assays for a definitive answer.

5. Conclusion

Taken together our data suggest that deficiency of SPOCK2 leads to differences in the bone phenotype, MSC physiology, as well as HSC number, inflammation and possible lymphocyte activation. However, the lack of mechanistic details underlying the bone and hematological phenotypes, the discrepancy of some of our bone-associated findings between female and male mice, the possible compensation by other SPOCK molecules to the observed findings, and the lack of verification of our findings with MSC- or HSC-specific KO of *Spock2* limit our study and will need to addressed in further studies.

CRediT authorship contribution statement

Rahul Kumar: Writing – original draft, Methodology, Investigation. **Subhadeep Das:** Investigation. **Wahyu Minka:** Investigation. **Celina Reiter:** Investigation. **Raquel Pereira:** Investigation. **Dominik Fuhrmann:** Resources, Investigation. **Richard Schneider:** Conceptualization. **Anita Seshire:** Methodology, Conceptualization. **Christof Reusch:** Methodology, Formal analysis. **Claire Conche:** Methodology. **Katharina Imkeller:** Investigation, Formal analysis. **Paola Divieti Pajevic:** Formal analysis, Conceptualization. **Daniela S. Krause:** Writing – review & editing, Supervision, Methodology, Funding acquisition, Formal analysis, Conceptualization.

Author contributions

R.K. and D.S·K designed the experiments. R.K., S. D., W.M., R.P. and C.R. performed the in vitro experiments. R.K. and W.M. performed the in vivo experiments. R.K. analyzed the data. C.R. performed the nanostring and the bioinformatic analyses. K.I. performed further bioinformatic analyses. C.C. performed the sorting of cells. P. D. P. analyzed the microCT data. R.S., A.S., P. D. P. provided input on experiments and critically reviewed the manuscript. R.K. wrote a first draft of the manuscript. D.S.K. supervised the research, analyzed data and wrote the manuscript.

Funding sources

This work was supported by Merck KGaA.

Declaration of competing interest

The authors declare that this work was supported by Merck KGaA. D. S.K. holds patents WO2018046666A1 - “Fibronectin or ILK inhibitors for use in the treatment of leukemia” and WO2020016346A1 - “Periostin compounds for the treatment of haematological complications”. R.K. holds patent WO2018046666A1 - “Fibronectin or ILK inhibitors for use in the treatment of leukemia”.

Acknowledgements

This work was financially supported by Merck KGaA. The microCT was partially supported by the Massachusetts General Hospital, Center for Skeletal Research (CSR), an NIH-funded program (P30 AR075042), which is supported by NIAMS. We thank Taconic Biosciences for generating the SPOCK2 KO mice. K. I. was supported by the Mildred Scheel Center Frankfurt (German Cancer Aid).

Appendix A. Supplementary data

Supplementary data to this article can be found online at https://doi.org/10.1016/j.bone.2025.117539.

Data availability

For original data, please contact the corresponding author.

References

[1] F. Notta, S. Zandi, N. Takayama, S. Dobson, O.I. Gan, G. Wilson, K.B. Kaufmann, J. McLeod, E. Laurenti, C.F. Dunant, J.D. McPherson, L.D. Stein, Y. Dror, J.E. Dick, Distinct routes of lineage development reshape the human blood hierarchy across ontogeny, Science 351 (6269) (2016) aab2116, https://doi.org/10.1126/science.aab2116.
[2] S. Méndez-Ferrer, et al., Bone marrow niches in haematological malignancies, Nat. Rev. Cancer 20 (2020) 285–298.
[3] Kumar, R., Godavarthy, P. S., Krause, D. S. The bone marrow microenvironment in health and disease at a glance. J. Cell Sci., 131, pii: jcs201707 (2018).
[4] T. Itkin, et al., Distinct bone marrow blood vessels differentially regulate haematopoiesis, Nature 532 (2016) 323–328.
[5] A. Ludin, et al., Reactive oxygen species regulate hematopoietic stem cell self-renewal, migration and development, as well as their bone marrow microenvironment, Antioxid. Redox Signal. 21 (2014) 1605–1619.
[6] C. Frantz, K.M. Stewart, V.M. Weaver, The extracellular matrix at a glance, J. Cell Sci. 123 (2010) 4195–4200.
[7] J.K. Mouw, G. Ou, V.M. Weaver, Extracellular matrix assembly: a multiscale deconstruction, Nat. Rev. Mol. Cell Biol. 15 (2014) 771–785.
[8] A.D. Bradshaw, E.H. Sage, SPARC, a matricellular protein that functions in cellular differentiation and tissue response to injury, J. Clin. Invest. 107 (2001) 1049–1054.
[9] C.H. Chang, et al., Secreted protein acidic and rich in cysteine (SPARC) enhances cell proliferation, migration, and epithelial mesenchymal transition, and SPARC expression is associated with tumor grade in head and neck Cancer, Int. J. Mol. Sci. 18 (2017).
[10] A.M. Delany, et al., Osteopenia and decreased bone formation in osteonectin-deficient mice, J. Clin. Invest. 105 (2000) 915–923.
[11] D. Ngo, et al., Circulating testican-2 is a podocyte-derived marker of kidney health, Proc. Natl. Acad. Sci. USA 117 (2020) 25026–25035.
[12] A. Hadchouel, et al., Overexpression of Spock2 in mice leads to altered lung alveolar development and worsens lesions induced by hyperoxia, Am. J. Phys. Lung Cell. Mol. Phys. 319 (2020) L71–l81.
[13] A. Schnepp, P. Komp Lindgren, H. Hülsmann, S. Kröger, M. Paulsson, U. Hartmann, Mouse testican-2. Expression, glycosylation, and effects on neurite outgrowth, J. Biol. Chem. 280 (12) (2005) 11274–11280, https://doi.org/10.1074/jbc.M414276200.
[14] A. Krajnc, A. Gaber, B. Lenarčič, M. Pavšič, The central region of Testican-2 forms a compact Core and promotes cell migration, Int. J. Mol. Sci. 21 (2020).
[15] M. Yang, et al., Angiogenesis-related genes may be a more important factor than matrix metalloproteinases in bronchopulmonary dysplasia development, Oncotarget 8 (2017) 18670–18679.
[16] A. Hadchouel, et al., Identification of SPOCK2 as a susceptibility gene for bronchopulmonary dysplasia, Am. J. Respir. Crit. Care Med. 184 (2011) 1164–1170.
[17] J. Zhao, et al., SPOCK2 serves as a potential prognostic marker and correlates with immune infiltration in lung adenocarcinoma, Front. Genet. 11 (2020) 588499.
[18] Y. Liu, X. Fan, C. Jiang, S. Xu, SPOCK2 and SPRED1 function downstream of EZH2 to impede the malignant progression of lung adenocarcinoma in vitro and in vivo, Hum. Cell 36 (2023) 812–821.

[19] U. Aghamaliyev, et al., SPOCK2 gene expression is downregulated in pancreatic ductal adenocarcinoma cells and correlates with prognosis of patients with pancreatic cancer, J. Cancer Res. Clin. Oncol. 149 (2023) 9191–9200.
[20] M. Jiao, W. Sun, L. Li, C. Li, J. Zhou, Q. Li, L. Duan, Clinical significance of SPOCK2 expression signature for high-grade serous ovarian cancer patients, Front. Genet. 13 (2022) 878123, https://doi.org/10.3389/fgene.2022.878123.
[21] O.J. Sansom, F.C. Mansergh, M.J. Evans, J.A. Wilkins, A.R. Clarke, Deficiency of SPARC suppresses intestinal tumorigenesis in APCMin/+ mice, Gut 56 (2007) 1410–1414.
[22] R. Kumar, R.S. Pereira, J. Niemann, A.I. Azimpour, C. Zanetti, C. Karantanou, W. Minka, V.R. Minciacchi, E. Kowarz, M. Meister, P.S. Godavarthy, V. Maguer-Satta, S. Lefort, E. Wiercinska, H. Bonig, R. Marschalek, D.S. Krause, The differential role of the lipid raft-associated protein flotillin 2 for progression of myeloid leukemia, Blood Adv. 6 (12) (2022) 3611–3624, https://doi.org/10.1182/bloodadvances.2021005992.
[23] V.R. Minciacchi, Christina Karantanou, Jimena Bravo, Raquel S. Pereira, Costanza Zanetti, Theresa Krack, Rahul Kumar, Katrin Bankov, Sylvia Hartmann, Brian J.P. Huntly, Eshwar Meduri, Wolfram Ruf, Daniela S. Krause, Differential inflammatory conditioning of the bone marrow by acute myeloid leukemia and its impact on progression, Blood Adv. 8 (19) (2024) 4983–4996, https://doi.org/10.1182/bloodadvances.2024012867.
[24] J.C. Wheat, et al., The corepressor Tle4 is a novel regulator of murine hematopoiesis and bone development, PLoS One 9 (2014) e105557.
[25] A. Subramanian, et al., Gene set enrichment analysis: a knowledge-based approach for interpreting genome-wide expression profiles, Proc. Natl. Acad. Sci. USA 102 (2005) 15545–15550.
[26] G. Yu, L.G. Wang, Y. Han, Q.Y. He, clusterProfiler: an R package for comparing biological themes among gene clusters, Omics 16 (2012) 284–287.
[27] D.D. Houlihan, et al., Isolation of mouse mesenchymal stem cells on the basis of expression of Sca-1 and PDGFR-α, Nat. Protoc. 7 (2012) 2103–2111.
[28] M. Iliopoulou, et al., Extracellular matrix rigidity modulates physical properties of subcapsular sinus macrophage-B cell immune synapses, Biophys. J. 123 (2024) 2282–2300.
[29] J. Song, et al., Extracellular matrix of secondary lymphoid organs impacts on B-cell fate and survival, Proc. Natl. Acad. Sci. USA 110 (2013) E2915–E2924.
[30] S. Mendez-Ferrer, D. Lucas, M. Battista, P.S. Frenette, Haematopoietic stem cell release is regulated by circadian oscillations, Nature 452 (2008) 442–447.
[31] S. Méndez-Ferrer, et al., Mesenchymal and haematopoietic stem cells form a unique bone marrow niche, Nature 466 (2010) 829–834.
[32] L. Ding, T.L. Saunders, G. Enikolopov, S.J. Morrison, Endothelial and perivascular cells maintain haematopoietic stem cells, Nature 481 (2012) 457–462.
[33] E.S. Novoseletskaya, P.V. Evdokimov, A.Y. Efimenko, Extracellular matrix-induced signaling pathways in mesenchymal stem/stromal cells, Cell Commun. Signal 21 (2023) 244.
[34] X.D. Chen, Extracellular matrix provides an optimal niche for the maintenance and propagation of mesenchymal stem cells, Birth Defects Res. C Embryo Today 90 (2010) 45–54.
[35] S. Becerra-Bayona, V. Guiza-Arguello, X. Qu, D.J. Munoz-Pinto, M.S. Hahn, Influence of select extracellular matrix proteins on mesenchymal stem cell osteogenic commitment in three-dimensional contexts, Acta Biomater. 8 (2012) 4397–4404.
[36] S. Mathews, R. Bhonde, P.K. Gupta, S. Totey, Extracellular matrix protein mediated regulation of the osteoblast differentiation of bone marrow derived human mesenchymal stem cells, Differentiation 84 (2012) 185–192.
[37] C. Popov, et al., Integrins α2β1 and α11β1 regulate the survival of mesenchymal stem cells on collagen I, Cell Death Dis. 2 (2011) e186.
[38] D.Y. Yuh, et al., The secreted protein DEL-1 activates a β3 integrin-FAK-ERK1/2-RUNX2 pathway and promotes osteogenic differentiation and bone regeneration, J. Biol. Chem. 295 (2020) 7261–7273.
[39] J. Lam, et al., TNF-alpha induces osteoclastogenesis by direct stimulation of macrophages exposed to permissive levels of RANK ligand, J. Clin. Invest. 106 (2000) 1481–1488.
[40] K. Kobayashi, et al., Tumor necrosis factor alpha stimulates osteoclast differentiation by a mechanism independent of the ODF/RANKL-RANK interaction, J. Exp. Med. 191 (2000) 275–286.
[41] R. Liao, et al., Interleukin-1 induces receptor activator of nuclear factor-κB ligand-independent osteoclast differentiation in RAW264.7 cells, Exp. Ther. Med. 21 (2021) 640.
[42] C. Zanetti, D.S. Krause, "caught in the net": the extracellular matrix of the bone marrow in normal hematopoiesis and leukemia, Exp. Hematol. 89 (2020) 13–25.
[43] N. Alcorta-Sevillano, I. Macías, A. Infante, C.I. Rodríguez, Deciphering the relevance of bone ECM signaling, Cells 9 (2020).
[44] A. Bentmann, et al., Circulating fibronectin affects bone matrix, whereas osteoblast fibronectin modulates osteoblast function, J. Bone Miner. Res. 25 (2010) 706–715.
[45] F.C. Mansergh, et al., Osteopenia in Sparc (osteonectin)-deficient mice: characterization of phenotypic determinants of femoral strength and changes in gene expression, Physiol. Genomics 32 (2007) 64–73.
[46] N. Kajitani, T. Yamada, K. Kawakami, K.I. Matsumoto, TNX deficiency results in bone loss due to an increase in multinucleated osteoclasts, Biochem. Biophys. Res. Commun. 512 (2019) 659–664.
[47] K.H. Susek, et al., Bone marrow laminins influence hematopoietic stem and progenitor cell cycling and homing to the bone marrow, Matrix Biol. 67 (2018) 47–62.
[48] Y.C. Gu, et al., Laminin isoform-specific promotion of adhesion and migration of human bone marrow progenitor cells, Blood 101 (2003) 877–885.
[49] F. Wirth, A. Lubosch, S. Hamelmann, I.A. Nakchbandi, Fibronectin and its receptors in hematopoiesis, Cells 9 (2020).
[50] A. Ehninger, et al., Loss of SPARC protects hematopoietic stem cells from chemotherapy toxicity by accelerating their return to quiescence, Blood 123 (2014) 4054–4063.
[51] K. Siva, et al., SPARC is dispensable for murine hematopoiesis, despite its suspected pathophysiological role in 5q-myelodysplastic syndrome, Leukemia 26 (2012) 2416–2419.

Glossary

Bone marrow microenvironment (BMM): *The complex network of cellular and acellular components inside the bone marrow that regulates normal and malignant hematopoiesis.:*
Hematopoiesis: *The process by which the hematopoietic stem cells inside the bone marrow produce and replenish different cellular components of the blood.:*
Mesenchymal stromal cells *(MSC): Vital components of the BMM, which can differentiate into adipocytes, chondrocytes and osteoblasts.:*
Extracellular matrix (ECM): *A network of bioactive components, including proteins such as fibronectin or SPOCK2. This network is essential for the adhesion, migration and signaling between cells.:*
Hematological phenotyping: *The examination of different cell types in the peripheral blood, bone marrow and spleen. These blood cells include, amongst others, hematopoietic stem cells, multipotent progenitors, megakaryocytes, B cells, T cells, myeloid cells etc.:*
Colony formation: *The property of hematopoietic stem cells (HSC) or MSC to produce viable colonies when cultured in methylcellulose with appropriate cytokine supplementation. This is a measure of the clonogenic potential of cells.:*
Microcomputed tomography: *An imaging method that uses X-rays to reveal the architecture of bone. This method can also be used to quantify the bone volume and bone thickness.:*
Tartrate-Resistant Acid Phosphatase (TRAP) staining: *A staining method to detect tartrate-resistant acid phosphatase-positive cells which represent bone-resorbing cells, osteoclasts.:*